



Near-infrared spectroscopy and machine learning for classification of food powders during a continuous process

Samet Ozturk^{a,b,**}, Alexander Bowler^a, Ahmed Rady^a, Nicholas J. Watson^{a,*}

^a Food, Water, Waste Research Group, Faculty of Engineering, University of Nottingham, University Park, Nottingham, UK

^b Department of Food Engineering, Gümüşhane University, Gümüşhane, Turkey

ARTICLE INFO

Keywords:

Food powders
Near-infrared spectroscopy
In-line sensors
Machine learning
Digital manufacturing.

ABSTRACT

In food production environments, the wrong powder material is occasionally loaded onto a production line which impacts food safety, product quality, and production economics. The aim of this study was to assess the potential of using Near Infrared (NIR) spectroscopy combined with Machine Learning to classify food powders under motion conditions. Two NIR sensors with different wavelength ranges were compared and the ML models were tasked with classifying between 25 food powder materials. Eleven different spectra pre-processing methods, three feature selection methods, and five algorithms were investigated to find the optimal ML pipeline. It was found that pre-processing the spectra using autoencoders followed by using support vector machines with the all spectral wavelengths from both sensors was most accurate. The results were improved further using under-sampling and boosting. Overall, this method achieved 99.52, 97.12, 94.08, and 91.68% accuracy for the static, 0.017, 0.036 and 0.068 m s⁻¹ sample speeds. The models were also validated using an independent test sets.

1. Introduction

Food powders including flours, spices, nut or animal derived, play an important role in the production of many food products (Su and Sun, 2018). The quality and safety of these food powders have a significant impact on human health. Therefore, measurements related to chemical composition (e.g., starch or protein content) (Yang et al., 2013), adulteration (such as species or origin) (Lohumi et al., 2014), mycotoxin content (such as aflatoxins) (Teena et al., 2014), allergen content (Laborde et al., 2020) or parasitic infection (e.g., red flour beetles or weevils) (Campbell and Arbogast, 2004) are required for quality and safety assurance throughout food production. Previous studies have shown that the most common foods linked to allergen incidents tend to be prepared dishes, snacks, cereals, bakery, and confectionary (FSA, 2020). These foods are typically more complex as they usually contain a large number of ingredients and are often produced using more complicated processes causing more scope for mistakes. Human errors such as using the wrong ingredient (many powdered food materials have similar appearance) or mislabelling of materials can result in food safety and quality incidents. These kinds of problems may appear unlikely but a

2019 UK workshop on food allergens and safety, which included a range of food production stakeholders (manufacturers, regulators, technology providers and academics), concluded that the largest risk to cross-contamination of powdered foods was mislabelling or accidental misuse of materials within production environments (Pauli et al., 2020). In 2020, the Food Standard Agency also reported that 18% of all failures resulting in allergy alerts were production errors associated with either formulation/assembly errors or work in progress labelling errors (FSA, 2020). Therefore, for early detection of these problems, techniques to monitor or confirm the composition of food in production environments in real-time are required. Optical spectroscopic technologies have been developed to monitor the origin of food products for industrial and laboratory-based applications (Damez and Clerjon, 2013; Su and Sun, 2017). Among them, NIR spectroscopy offers many advantages including composition analysis under sample movement, non-destructive measurement and little or no sample preparation. These advantages make it convenient for in-line applications in a processing plant compared to traditional methods such as Approximate Analysis, High Performance Liquid Chromatography (HPLC), or Mass Spectroscopy (MS) (Salguero-Chaparro et al., 2013; Zamora-Rojas et al., 2012). NIR spectroscopy

* Corresponding author.

** Corresponding author.

E-mail addresses: sozturk@gumushane.edu.tr (S. Ozturk), Nicholas.Watson@nottingham.ac.uk (N.J. Watson).

measurements are based on the wave-absorption frequencies of chemical bonds within functional groups including C–H, O–H, N–H, and C=O, which are primarily related to the chemical composition and structure of materials (Silva et al., 2021). The evaluation of NIR spectroscopy for in-line conditions similar to industrial processes, such as on a moving conveyor belt or in a pilot scale production facility has been performed using a variety of food products including curd (Mateo et al., 2010), pears (Xu et al., 2012), olives (Salguero-Chaparro et al., 2013), potato chips (Pedreschi et al., 2010), fish fillets (ElMasry and Wold, 2008), brown rice (Li et al., 2013) and pasta (Temmerman et al., 2007).

Furthermore, recent studies have demonstrated applications of NIR on food powders (primarily flours and spices) to determine moisture content, particle size, micronutrients (carbohydrate, fat, and protein) and adulterant detection (Wang et al., 2022; Galvin-King et al., 2021; Modupalli et al., 2021; Porep et al., 2015) Li et al., 2013). These studies demonstrated that NIR techniques are capable of measuring surface and near surface (1–2 mm depth) properties in real time. However, the relationship between acquired NIR spectra and corresponding food powder properties is highly nonlinear with overlapping absorption bands due to the small spectral differences among foods with similar composition, which complicates spectral analysis (Chen and Wang, 2019a). Therefore, it is difficult to establish an accurate model to classify among the various food powders for in-line production. An automated process diagnosis requires suitable signal processing and interpretation for in-line industrial process monitoring. Supervised Machine Learning (ML) maps input data to output classes (classification) or values (regression) during training so that results can be predicted from new input data. ML allows functions to be fitted to input-output relationships without having to define the often-complicated underlying physical models. The accuracy of ML models is dependent on the input feature variables that are used in the model. Therefore, NIR spectroscopy coupled with ML algorithms has gained interest in process control, quality and safety applications within food powders (Liu et al., 2021; Zhou et al., 2020; dos Santos Pereira et al., 2021). Different ML algorithms including Support Vector Machines (SVMs), Artificial Neural Networks (ANNs), K-Nearest Neighbours (KNNs) and Convolutional Neural Networks (CNNs) have been successfully applied for analysing spectral data to monitor various food powders based on their origin, chemical composition and quality parameters (Mohamed et al., 2019; You et al., 2017). CNNs have become a popular ML algorithm due to their ability to automatically determine the important features of a signal or dataset without any human supervision (Napoletano et al., 2018). CNN models have been successfully applied for analysing visual imagery, facial recognition, language processing, age prediction and time series data (Chen et al., 2020; Chandler et al., 2019; Lussier et al., 2019). Recent studies have also shown the effectiveness of CNNs on the analysing spectral data for different purposes (Chen and Wang, 2019a; Zhou et al., 2020). CNNs were investigated in this study due to their advantage of automatic feature selection compared with the other ML algorithms. In most cases, obtained results have demonstrated a very positive impact of CNNs for classification models compared to other traditional ML models (Krauß et al., 2018). Although NIR and ML has been used to study food before, the vast majority of work measure static samples and are therefore not representative of the moving conditions of food powders in production lines.

The aim of this study is to evaluate the ability of NIR sensors combined with ML to classify different types of moving food powders. Specifically, the objectives are; 1) to classify many types of food powders, 2) determine the effect of speed on ML models, 3) determine the optimal pre-processing methods, feature selection techniques and ML algorithms for the given application 4) compare two NIR sensors with different wavelength ranges and the potential of combining data from the two sensors 5) Develop and assess models with an independent dataset.

2. Material and method

2.1. Sample preparation

A total of 25 powdered food materials (from 19 different origins) were investigated in this work to cover a range of typical materials used by the food sector. The some of these included allergens such as nuts and gluten. Food powders were obtained from different local stores in Nottingham, United Kingdom and are listed in Table 1. The same material type from different brands were also included to determine their effect on the acquired NIR spectra and performance of classification ML models. The composition and an image of each sample is provided in Supplementary Material Table 1.

2.2. NIR spectroscopy measurement

A schematic view of the measurement system used in this study is shown in Fig. 1. This system consists of portable NIR sensors fixed on a rotating system that connects to a desktop computer via USB cable. The NIR spectra of all food powders with different velocities (0–0.068 m/s) were recorded using NIRONE S2.0 and S2.5 sensors (Spectral Engines, Oulu, Finland). The S2.0 and S2.5 sensors have the same compact shapes with slightly different dimensions $25 \times 25 \times 17.5 \text{ mm}^3$ and $28 \times 25 \times 17.5 \text{ mm}^3$, and weights 15 g and 31 g, respectively. They consist of two tungsten vacuum lamps with a maximum power of 1 W and one element of InGaAs detectors. These sensors have a signal-to-noise ratio (SNR) of 38.75 dB. The detection ranges of each sensor are specified as 1550–1950 nm and 2000–2450 nm for S2.0 and S2.5, respectively, with 1 nm spectral resolution. Moreover, a reference spectrum was recorded using a white reference disk at 90% light intensity and a dark background measurement at 0% light intensity. The distance between the NIR sensor and sample surface was set as 2 cm to obtain a consistent measurement.

2.3. Moving stage

The experimental set up was designed so that the NIR sensors measured a single sample at a time. Samples of approximately 100 g were placed into a 12 cm diameter glass Petri dish and compressed to obtain a flat top surface. All samples were then scanned in both static and motion conditions. For the static mode, between replications, the sample holder was moved by hand under the NIR sensor to cover all multiple points on the sample surface. Then the measurements under motion were conducted using a rotational sample holder (Fig. 1) for the same sample. The tangential speeds were calculated using rotational speed and radial distance (4.65 cm) of the sensor from the centre of the rotating system and were 0.017, 0.036, and 0.068 m/s. For all static and in motion measurements, ten spectra were acquired from each sample. Five independent petri dishes of each sample were prepared. Then 10

Table 1
Food powders used for near-infrared (NIR) spectroscopy measurements.

Food Powders			
Flours Containing Gluten	Gluten-Free Flours	Nut Flours	Animal-Based Powders
Spelt Flour	Gluten-Free White Flour (three brands)	Peanut Flour	Whole Egg Powder
Rye Flour	Coconut Flour	Powdered Peanut Butter	Egg Yolk Powder
Buckwheat Flour	Tapioca Flour	Almond Flour (three brands)	Egg White Powder
Oat Flour	Corn Flour		
Barley Flour	Rice Flour		
Brown Flour			
Wheat Flour (three brands)			
Wheat Gluten			

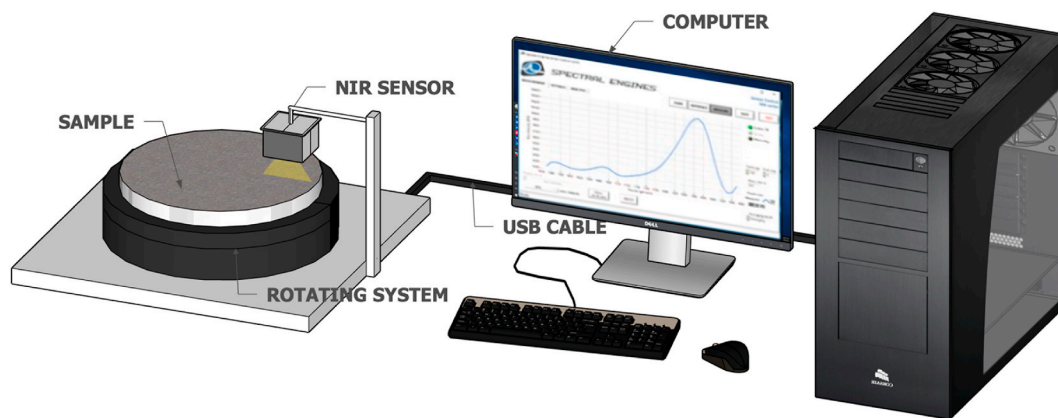


Fig. 1. A schematic view of experimental set-up for determining NIR spectra under different motion conditions.

spectra at different starting position (but same radial distance) were acquired from each Petri dish using both sensors. Overall, 50 independent spectra were obtained from 5 separate petri dishes of each sample.

2.4. Data modelling

ML models were developed to classify 19 different types of powdered food materials based on their origins. The data was divided into training, validation, and test instances. First, the test set was chosen as 50% of the data from each category of food powders using an interleaved method to select every other instance. Next, the remaining data was divided into 50% training and 50% validations sets using the same method to enable 2-fold cross validation. For evaluation on the test set, the models were trained using the training and validation sets combined. 50% train-test splits and 50% train-validation splits were chosen to allow determinations of the most generalisable ML pre-processing, feature selection, and algorithm pipeline. There were 625 spectra in the training and validation, and test sets. Separate modes for each speed were trained. I.e., for the stationary spectra, the ML models were trained using stationary spectra, and for the 0.017 m/s, the ML models were trained using the spectra acquired at this speed. In industrial application of a NIR sensor and ML combination, the number of samples measured will be much greater than the size of training data. Therefore, to get an accurate understanding of how well the ML methods are likely to perform

in practice, this large test and validation set sizes were chosen. Commonly, 5-fold validation is conducted where each validation set size is 20% of the total training and validation data, and the final test data is 20% of the total data (Kosmowski and Worku, 2018). However, this assumes that the whole data variation is contained within 20% of the data. Therefore, to increase confidence in the models, larger validation and test sizes were used in this study.

2.5. Spectral data pre-processing

A flow chart of the spectrum pre-processing, feature selection and ML algorithms used in this work is shown in Fig. 2. The effect of different spectral pre-processing methods on ML model classification accuracy was evaluated. The pre-processing methods investigated were mean centering, double centering, scaling, auto-scaling, robust auto-scaling, standard normal variate, Savitzky-Golay, first derivative smoothing, second derivative smoothing, multiplicative scatter correction (MSC) and autoencoders in addition to using the spectra without any pre-processing. Mean centering method subtracts the average spectral data of all food powder samples from the spectral data of each sample. This results in an average spectral matrix that has a value of zero, which effectively eliminates absolute absorption (Yan et al., 2020). The mean centered k th wavelength of the i th sample is defined by Eq. (1);

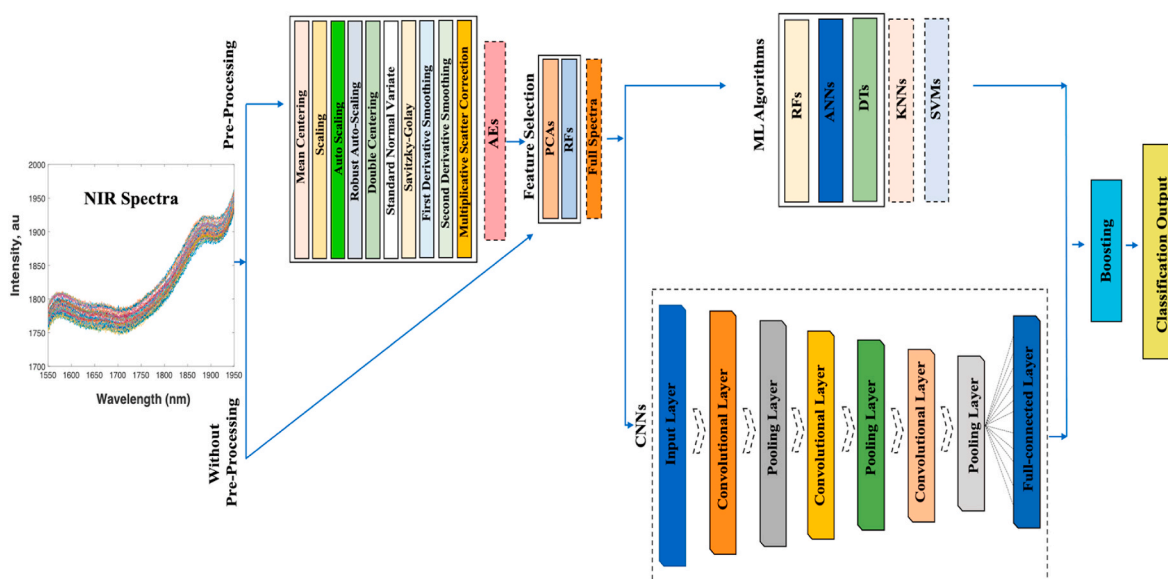


Fig. 2. A flow chart of spectral pre-processing, feature selection and machine learning algorithms.

$$x_{centered} = x - \frac{\sum_{k=1}^n x_{i,k}}{n} \quad \text{Eq. (1)}$$

where x is raw spectrum, n is the number of samples, $k = 1, 2, \dots, m$, m is the number of wavelength points. The scaling procedure was applied in cases where different spectra need to be scaled for comparison purposes. Scaling results in a spectrum with a mean of zero and a standard deviation of 1. Autoscaling was applied to compare food powders based on the correlations by using the standard deviation as the scaling factor (Rinnan et al., 2009). The first derivative smoothing method is applied to eliminate spectral baseline drift and effectively eliminate interference from baselines and other backgrounds (Adewale et al., 2014).

It is estimated as the difference between two subsequent measurement points as described in Eq. (2) and the second derivative smoothing provides smoothing using a fast method of adjacent calculating difference between two successive points of the first derivative spectra as following Eq. (3):

$$x'_i = x_i - x_{i-1} \quad \text{Eq. (2)}$$

$$x''_i = x'_i - x'_{i-1} = x_{i-1} - 2x_i + x_{i+1} \quad \text{Eq. (3)}$$

where x'_i indicates the first derivative and x''_i the second derivative at the point (wavelength) i (Rinnan et al., 2009). The interval for calculating the derivative was 1 nm.

The standard normal variate centres each spectra and divides by its standard deviation, so that the new spectra is centered on zero with a standard deviation of one. Savitzky-Golay smoothing is an effective method to eliminate spectral noise (Chen and Wang, 2019b). In this smoothing method, a moving window is fitted with polynomial least squares, and the smoothing effect changes according to the window width. The average value of spectrum of each sample pre-processed by Savitzky-Golay is calculated by

$$x_{k,smooth} = \bar{x}_k = \frac{1}{H} \sum_{i=-w}^{+w} x_{k+i} / h_i \quad (4)$$

Where x is raw spectrum, H is the normalization factor and h_i is the smoothing coefficient. To minimize the effect of smoothing on useful information, the measured value is multiplied by a smoothing factor of h_i . MSC was applied as a common pre-processing method for multi-wavelength calibration (Zhang et al., 2020) to eliminate the scattering effects caused by physical factors including particle size, loading density and moisture of samples. A polynomial order of 5 and a window length of 25 was chosen for the Savitzky-Golay filtering. It also enhances the signal to noise ratio. The specific computing steps were as follow;

Calculate the average spectrum of the calibration set samples

$$\bar{A}_{i,j} = \frac{\sum_{i=1}^n A_{i,j}}{n} \quad \text{Eq. (5)}$$

Where $\bar{A}_{i,j}$ refers to the average spectrum of the calibration set samples, n is the number of samples. i refers to the sample index where j refers to the wavelength index. Then Linear regression based on average spectrum was performed out by least square method;

$$A_i = m_i \bar{A} + b_i \quad \text{Eq. (6)}$$

Where A_i refers to the predicted spectrum for sample i , and m_i and b_i refers to regression constants. Then MSC-correlated spectrum was calculated by following;

$$A_{i(MSC)} = \frac{A_i - b_i}{m_i} \quad \text{Eq. (7)}$$

$A_{i(MSC)}$ refers to the corrected spectrum for sample i using the MSC method.

A polynomial order of 5 and a window length of 25 was chosen for

the Savitzky-Golay filtering. Autoencoders (AEs) are a neural network that attempts to reconstruct their inputs during training after passing through a bottleneck, or latent space. As noise in the spectra does not correlate with wavelength intensities it is not reconstructed by the network (Patel and Upla, 2022). The AEs used in this work had a latent space size of 100 and were trained for 3000 epochs using an L2 regularization penalty of 0.1 and the Scaled Conjugate Gradient training function.

To understand the difference between the recorded spectra of the different samples the spectral similarity was calculated for each sensor and the four different motion conditions. For these calculations, the average spectra for each material were obtained by averaging the intensities at each wavelength. Each of these new spectra were normalized to have a maximum intensity of one and minimum intensity of zero. The root mean square error of these spectra between each material were calculated. The errors were also scaled to have a maximum of one and a minimum of zero to aid comprehension. Therefore, values closer to zero indicate spectra that are similar, whilst values closer to one indicate spectra that are more diverse. These results for spectral similarity are available in supplementary materials Tables 2-9.

2.6. Feature selection

Three feature selection methodologies were investigated: 1) The full spectra, 2) Principal Component Analysis to extract 99.9% of the variance, and 3) RFs to choose the 30 wavelengths with the largest importance. PCA is an unsupervised ML method that linearly transforms input variables into uncorrelated outputs, or principle components (PCs) (Khalid et al., 2014). Feature importance and influential wavelength ranges can be determined using RFs by summing the error or impurity at every decision node in the trees (MATLAB, 2021). All experimental methods, including data pre-processing and ML algorithms were performed in MATLAB.

2.7. Machine learning algorithms

The majority of previous research that has utilised ML models to analyse spectroscopic measurements has been to determine whether a food powder was adulterated or to identify the type of food powder (Liu et al., 2021; You et al., 2019). According to Corro-Herrera et al. (2016), optimization methods are as accurate as each other for all possible problems based on the No Free Lunch theorem. Thus, the optimal algorithm is dependent on the specific application. In this study, five types of standard ML algorithms including DTs, RFs, KNN, ANN and SVMs were used, in addition to CNNs to determine the best model for in-line monitoring of food powders.

For classification tasks, SVMs consider a hyperplane that distinguishes two classes of data by maximizing the hyperplane's distance from the closest data points from each category. SVMs are effective with high dimensional feature spaces through the application of the kernel trick for non-linear fitting (Smola and Schölkopf, 2004). DTs apply conditions successively to input data until an output decision is reached. Their simplicity, interpretability, low computational cost, and ability to be graphical represented makes them more attractive than other algorithms, but they typically have lower accuracy (Rodriguez-Galiano et al., 2015). As an alternative, RFs combine the predictive performance of multiple DTs by selecting, for example, the most common class predicted in classification tasks (Escrig et al., 2020). To determine the class of the queried new point, KNN calculates the distance between data points in the feature space and use a voting procedure of the K closest training instances (Escrig et al., 2019). The hidden layers of ANNs can create combinations of input features to nonlinearly fit model inputs to outputs. Weights and bias terms connect the inputs to successive layers in the network until an output is reached. The use of CNNs in image recognition is extremely popular because of their ability to automatically learn spatially variant features important to the task (Munir et al., 2017). CNNs consist

Table 2

The hyperparameters used in this study and a literature review of hyperparameters used for CNNs combined with NIR spectra.

Hyperparameter	In this study	Previous studies	References
Number of convolutional layers	4	1	Yan et al., 2020; Zhou et al., 2020; Cui and Fearn, 2018
		2	(Einarson et al., 2022)2; Tsakiridis et al., 2020
		3	Wang et al., 2020; Ma et al. (2021); Liu et al. (2021)
		4	Wang et al., 2020; Kawamura et al. (2021); Tegegn et al. (2021)
Dropout	0.5	0.3	Tegegn et al. (2021)
Epochs	1000	0.4	Kawamura et al. (2021)
		100	Ng et al., 2020; Tegegn et al. (2021)
		300	(Einarson et al., 2022)2
		750	Mishra et al., 2021
		1000	Tsakiridis et al. (2020)
Conv 1 filters	16	16	Liu et al. (2021)
		24	Tsakiridis et al. (2020)
		32	Kawamura et al. (2021); Tegegn et al. (2021); Ng et al., 2020
		36	Cui and Fearn (2018)
		128	Ma et al. (2021)
Conv 2 filters	32	16	Liu et al. (2021)
		32	Tegegn et al. (2021)
		48	Tsakiridis et al. (2020)
		64	Ng et al., 2020; Tsakiridis et al., 2020
		256	Ma et al. (2021)
Conv 3 filters	64	16	-(Liu et al., 2021)
		64	Tegegn et al. (2021)
		128	Ma et al. (2021); Tsakiridis et al., 2020; Ng et al., 2020
Conv 4 filters	128	64	Tegegn et al. (2021)
		256	Kawamura et al. (2021); Ng et al., 2020
Conv 1 filter size	9, dilation factor of 2	3	Tegegn et al. (2021)
		5	Liu et al. (2021); Cui and Fearn, 2018;
		7	Tsakiridis et al. (2020)
		8	Ma et al. (2021)
		9	Wang et al. (2020)
		20	Ng et al., 2020; Kawamura et al. (2021)
		3	Tegegn et al. (2021)
		5	Wang et al., 2020; Ma et al. (2021); Liu et al. (2021)
		7	Tsakiridis et al. (2020)
Conv 3 filter size	7	20	Ng et al., 2020; Kawamura et al. (2021)
		3	Ma et al. (2021); Tegegn et al. (2021)
		5	Wang et al., 2020; Liu et al. (2021)
		7	Wang et al. (2020)
		20	Wang et al., 2020; Kawamura et al. (2021)
Conv 4 filter size	7	3,7	Tegegn et al. (2021)
			Wang et al. (2020)
		20	Ng et al., 2020; Kawamura et al. (2021)
Neurons FC layer	32	32	Wang et al. (2020)
		100	Ng et al., 2020; Kawamura et al. (2021)
		512	Tegegn et al. (2021)
		10	Ng et al. (2020)
Batch size	8	32	Yan et al. (2020)
		256	Ng et al., 2020; Cui and Fearn, 2018
			Wang et al., 2020; (Yan et al., 2020)Y
			Cui and Fearn (2018)
Regularization	Varied between 0.01 and 0.1. Decided using single-fold validation	0.001, 0.005	Liu et al. (2021)
Learning rate	0.0001 Drop factor of 0.33 every 300 epochs	0.0001, 0.001, 0.01, 0.1	Ng et al., 2020; Tegegn et al. (2021)
Optimization function	Adam	Adam	Wang et al., 2020; (Yan et al., 2020); Cui and Fearn, 2018
Padding	“Same”	“Same”	Zhou et al. (2020)
Max pooling kernel size	2	2	(Einarson et al., 2022; Yan et al., 2020); ; Ng et al., 2020
Max pooling stride	2	1, 2, 3	Wang et al., 2020; (Yan et al., 2020); Liu et al. (2021)
Activation function	ReLU	ReLU	Ng et al., 2020; Kawamura et al. (2021)
			Wang et al. (2020)
			Wang et al. (2020)
			(Einarson et al., 2022); Yan et al., 2020; Kawamura et al. (2021)

of convolution layers, pooling layers, nonlinear activations and dense layers. Convolutional layers consist of filters that perform cross-correlation on the input data. For all investigations, the hyperparameters for the ML algorithms were optimized using the Bayesian Optimization Algorithm available in MATLAB. All eligible parameters were optimized for 30 iterations using the “expected improvement per second plus” acquisition function and 2-fold cross-validation. Preliminary investigations combined with a thorough literature review

determined the hyperparameters to use for the CNNs in Table 2. The L2 regularization parameter was chosen through 2-fold cross-validation.

2.8. Under sampling and boosting

After the optimal pre-processing, feature selection, and algorithm type were determined, under sampling and boosting were used to improve overall model accuracy, improve model accuracy on difficult

Table 3

Pre-processing results of S2.0 sensor at static mode for five types of ML algorithms. The bolded text highlights the highest, or joint-highest, accuracy models for each task.

Pre-processing method	Validation Set Accuracy				
	DT	RF	KNN	ANN	SVM
No pre-processing	0.8045	0.8878	0.9776	0.9776	0.9744
Mean centring	0.7981	0.8814	0.9647	0.984	0.9744
Scaling	0.8045	0.891	0.9615	0.984	0.9744
Auto scaling	0.8077	0.8654	0.9647	0.9744	0.9487
Robust auto scaling	0.8077	0.8718	0.9391	0.9872	0.9679
Double centring	0.7981	0.8622	0.9615	0.984	0.9744
Standard normal variate	0.7436	0.891	0.8526	0.9359	0.9231
Savitzky-Golay	0.8654	0.9103	0.9808	0.9776	0.9904
First derivative smoothing	0.7532	0.7821	0.8301	0.8237	0.8686
Second derivative smoothing	0.6474	0.7532	0.3269	0.4295	0.7276
Multiplicative scatter correction	0.6474	0.7821	0.8526	0.8237	0.8686
Autoencoders	0.8751	0.9487	0.9842	0.9808	0.984

to categorize materials, and provide a model confidence score for each prediction. Under sampling was used to decrease the dataset size of easily classified materials to give larger influence on more difficult categories during both model training and hyperparameter optimization. Boosting was used as an ensemble method to combine classifiers which were successively trained on datasets giving larger influence on previously poorly classified categories (Wang et al., 2020; Avila et al., 2018). Overall, five classifiers were combined through majority voting giving a final prediction along with a distribution of predictions which provides a measure of model confidence. For industrial application of NIR sensors and ML combinations, ensemble voting procedures can increase trust in the model predictions by providing a score of overall uncertainty in the prediction. For example, instances where predictions from multiple classifiers are not in agreement can indicate to operators that a sample should be taken and analysed off-line, or that more data for this particular class should be collected and the models retrained.

Table 4

Evaluation of feature selection methodologies using 5-fold cross validation for S2.0 sensor at the static mode. The bolded text highlights the highest, or joint-highest, accuracy models for each task.

Features Selection Methods	Validation Set Accuracy				
	DT	RF	KNN	ANN	SVM
Full Spectra	0.875	0.9487	0.984	0.9808	0.984
PCA	0.9295	0.9455	0.9808	0.9808	0.9647
RF	0.9167	0.9519	0.9776	0.9808	0.9808

Table 5

The most important wavelengths in order found using Random Forest (RF) algorithm at static spectra.

Wavelength (nm)	2051	2056	2060	2058	2064	2028	2307	2050	2029	2063	2312
Importance	1	0.73316	0.715927	0.548199	0.545683	0.465842	0.446842	0.321916	0.320133	0.308169	0.307874

Table 6

Test set classification accuracy for different ML algorithms and sensors. The bolded text highlights the highest, or joint-highest, accuracy models for each task.

Motion Mode	Test Set Accuracy									
	S2.0			S2.5			Combined			
	KNN	SVM	CNN	KNN	SVM	CNN	KNN	SVM	CNN	KNN
Static	0.9824	0.9872	0.9888	0.9984	0.9968	0.984	0.9936	0.9952	0.9808	0.984
0.017 m s ⁻¹	0.9264	0.9712	0.9584	0.8281	0.8943	0.8546	0.936	0.9696	0.8752	0.9168
0.036 m s ⁻¹	0.712	0.8896	0.8898	0.8565	0.8707	0.8598	0.9152	0.9392	0.8944	0.9328
0.068 m s ⁻¹	0.7376	0.8064	0.848	0.8254	0.7841	0.8162	0.9104	0.9152	0.8784	0.9392

2.9. Independent dataset analysis

Finally, to further understand model accuracy, the best ML pipeline was evaluated on test sets comprised of independent samples to the training and validation sets.

3. Results and discussion

3.1. Spectral features

Fig. 3 shows the representative raw mean NIR spectra of the 19

Table 7

The effect of boosting on the test set accuracy under all motion conditions for S2.0 sensor.

Motion Mode	Test Set Accuracy	
	Before boosting	After boosting
Static	0.9952	0.9952
0.017 m s ⁻¹	0.9696	0.9712
0.036 m s ⁻¹	0.9392	0.9408
0.068 m s ⁻¹	0.9152	0.9168

Table 8

The misclassified materials from the test set and S2.0 sensor at 0.068 m s⁻¹ and boosting. Classification accuracy for this model was 0.9168 (Table 7).

True Class	Predicted Class	Frequency
Rye flour	Barley flour	15
Barley flour	Rye flour	12
Buckwheat flour	Wheat flour	5
Wheat flour	Brown flour	4
Brown flour	Wheat flour	3
Whole egg powder	Peanut butter powder	3
Buckwheat flour	Barley flour	2
Gluten free white flour	Wheat flour	2
Peanut butter powder	Oat flour	2
Peanut butter powder	Tapioca flour	1
Spelt flour	Buckwheat flour	1
Wheat flour	Rye flour	1
Wheat flour	Spelt flour	1

Table 9

Independent dataset for training and validation of developed models.

Training and Validation Set Size (%)	Static Mode	0.017 m/s	0.036 m/s	0.068 m/s
40	0.993	0.841	0.808	0.8373
60	0.998	0.882	0.832	0.821
80	0.996	0.972	0.968	0.932

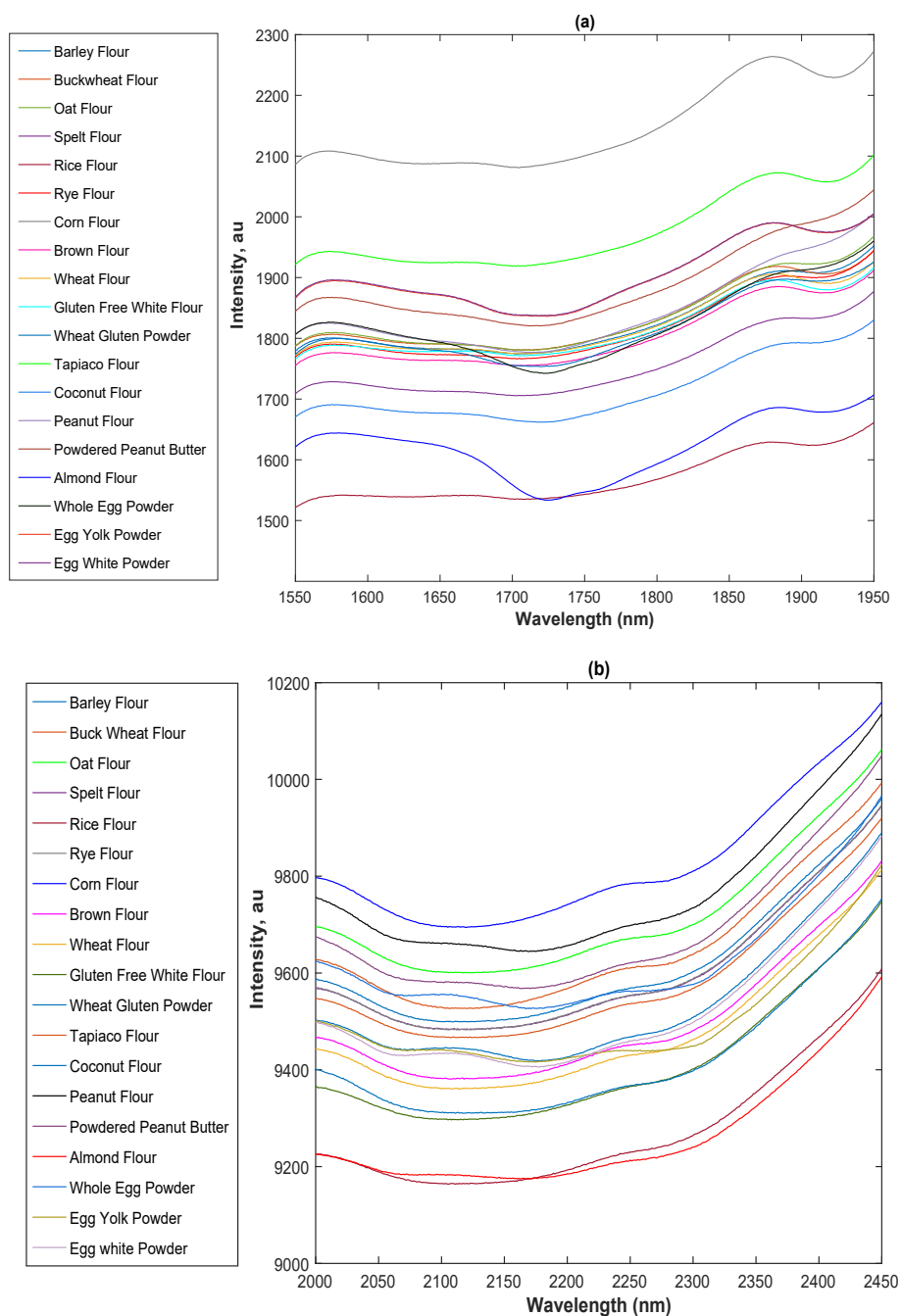


Fig. 3. The raw mean near infrared (NIR) spectra of all food powders acquired from S2.0 (a) and S2.5 (b) sensors at static conditions.

different food powders acquired from the S2.0 and S2.5 sensors of wavelength ranging from 1550 to 1950 nm and 2000–2450 nm respectively, in the static mode. The obtained NIR spectra revealed the principal absorptions bands corresponding to functional vibration of chemical bonds in the main food powders constituents (Fig. 3). As can be seen from the figures, the obtained spectra of most food powders are clearly distinguishable from the each other, but, some do overlap due to similar constituent content such as protein, carbohydrate, fat, or water as reported in previous studies (Rady et al., 2019; Cama-Moncunill et al., 2016). The first absorption band, approximately from 1550 to 1600 nm is related to O–H stretching of the first overtone in carbohydrates as reported for powdered infant formula by Cama-Moncunill et al. (2016). The protein absorption band for food powders in this study were at approximately 2150–2200 nm and can be attributed to the combination of C–O stretching, N–H bending and C–N stretching as previously

reported for wheat flour, peanut flour and dairy powders by Pu et al. (2021), Vitelli et al. (2021) and Mishra et al., 2015. Additionally, the water absorption bands due to the vibration of O–H bonds during NIR measurements were clearly seen for most food powders from 1900 to 1950 nm and from 2210 to 2400 nm, although some of them overlapped each other due to the similar moisture levels or other similar constituents. Rady et al., 2019 and Mishra et al., 2015 also reported similar absorbance regions between 1550 and 2450 nm for a wide variety of food powders including peanut flour and gluten free flours. Absorbance peaks in the range of 1720–1750 nm and 2100–2200 nm in the whole egg powder, egg yolk powder, powdered peanut butter, peanut flour, coconut flour and almond flour can be related to the presence of long-chain fatty acids which produce a CH_2 first overtone at 1725–1750 nm and 2100–2200 nm as recently shown in peanut flour and plant-based oils (Vitelli et al., 2021; Li et al., 2020). The spectral profiles

for the same samples including gluten containing wheat flour, gluten free wheat flour and almond flour from different brands looked similar except for the slightly visible differences in their absorption intensities, most probably due to their raw material origins (Fig. 3). Overall, the obtained spectra showed a good agreement with previous studies for the classification of similar food powders including peanut flour, corn flour and tapioca flour (Rady et al., 2019; You et al., 2019), dairy powders (Pu et al., 2021) and wheat flour (Vitelli et al., 2021) under static conditions.

3.2. Impact of the speed on the NIR spectra

To determine the impact of speed on the acquired data quality, the raw reflectance values (in intensity unit) of rye flour under static and motion conditions are shown in Figs. 4 and 5 for both the S2.0 and S2.5 sensors. As seen in Figs. 4 and 5, the acquired spectral absorption peaks for rye flour during the NIR measurement under motion conditions were in the same wavelength range as that of static mode. However, an increased level of noise was observed in the both spectra under motions conditions (Figs. 4–5), which could be attributed to a slight variation in the amount of reflected light detected by the NIR sensors, while the samples were in motions. Previous studies have reported increased variability when recording spectra from samples in linear motion with some common reasons including noise, data acquisition time, sample surface flatness or variable height between sample surface and sensor for variety of food products (Rady et al., 2019; Dixit et al., 2017; Munir et al., 2017).

The current study also identified the similar effect for rotating systems where the variability across recorded spectra of the same sample increased with rotational speed for both sensors. These results were in line with another study (Cama-Moncunill et al., 2016) that reported the effect of rotational speed on variance in the acquired NIR spectrum of

infant formula. However, more powerful spectral acquisition (150 W) systems have shown good spectral quality in detecting the absorption peaks for fat, protein, carbohydrate or allergen content of food powders over the range 1550–2450 nm under rotational and linear movements (Xia et al., 2018). Although motion conditions were employed to simulate real world food powder processing conditions, it should be noted that the lower speed capacity of rotating system may not be representative of faster operations such as process feeding or mixing lines on a conveyor belt. These operations would require higher power sensors which enable faster acquisition and reduce the noises and variances in the obtained spectra under motion conditions. Overall, the capability of low cost portable NIR sensors along with the ability to perform measurements under motion conditions illustrated a promising potential to be used as an in-line identification tool for the various food powders commonly used in the industry.

4. Classification results

4.1. Selecting spectra pre-processing method for ML algorithms

Table 3 summarizes the performance of the pre-processing methods evaluated on the validation set from S2.0 sensor at the static mode for five types of ML algorithms using the full spectra as input features. The bolded text highlights the highest accuracy models for each task. To determine the best pre-processing method to extract the most spectral information, the S2.0 sensor was chosen as more absorption peaks of chemical components fall within its wavelength range (Fig. 3a) and the samples at static mode were chosen due to less variation in the spectra (Fig. 4).

Overall, AEs pre-processing produced the most accurate classification models, achieving the highest classification accuracies for 3 out of 5

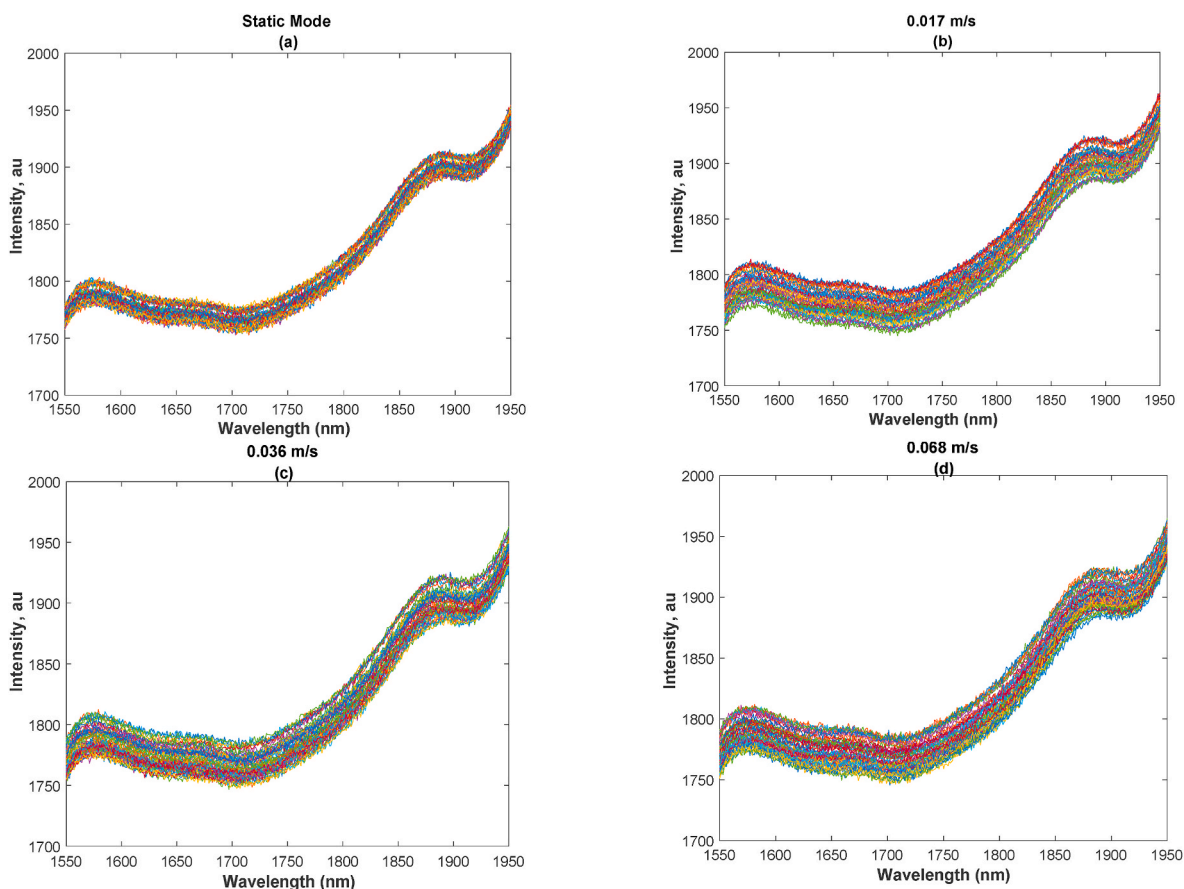


Fig. 4. Near infrared (NIR) spectra (50) of rye flour acquired from S2 sensor a) in static mode; b) at 0.017 m/s; c) 0.036 m/s; and d) 0.068 m/s.

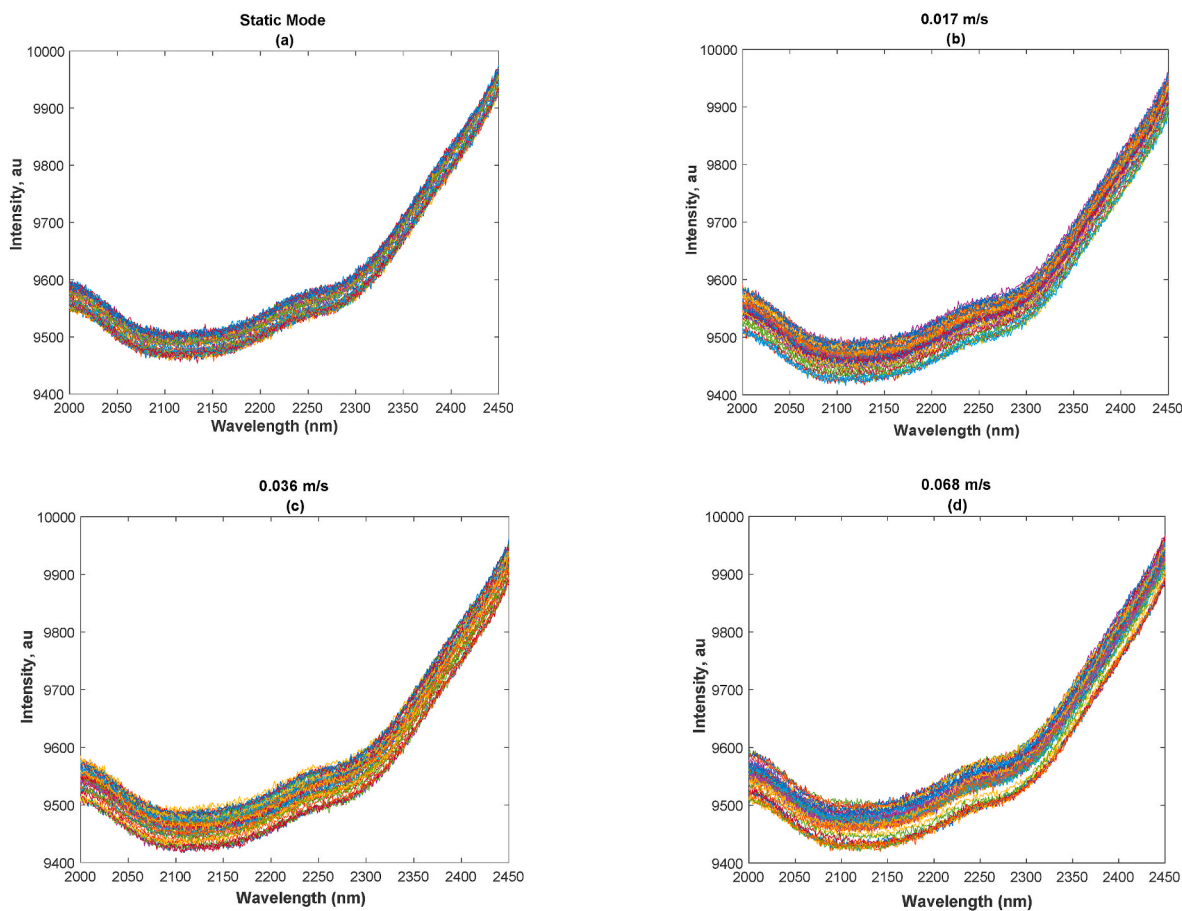


Fig. 5. Near infrared (NIR) spectra (50) of rye flour acquired from S2.5 sensor a) in static mode; b) at 0.017 m/s; c) 0.036 m/s; and d) 0.068 m/s.

ML algorithms when compared to the other methods (Table 3). Therefore, AEs were taken forward as the pre-processing method for all further investigations, including evaluation of feature selection methods, training CNNs, and final evaluation of models on the test sets in this study. The AEs pre-processed NIR spectra (50) of rye flour acquired using the S2.0 sensor under static conditions as a representative

example for all samples is shown in Fig. 6. The efficiency of AEs as a pre-processing method for NIR spectra datasets has also been shown in previous classification and prediction studies for real-time monitoring of solids and milk properties (Sharma et al., 2021; Sadeghi Vasafi and Hitzmann, 2021).

4.2. Feature selection evaluation

Overall, using the full spectra from the S2.0 sensor with KNNs and SVMs models at static mode produced the highest classification accuracy of 0.9808 compared to the other ML algorithms (all models except one had a classification accuracy above 0.915) (Table 4). Feng et al. has found the highest modelling accuracy when applying KNN and SVM to enhance the prediction accuracy for the classification of the variety of rice from different regions in the China using a dataset acquired from Raman Spectroscopy (Feng et al., 2013). This indicates that all the information from the spectra is required to classify each material. In contrast, PCA only extracts linear relationships between wavelengths, thereby eliminating non-linear trends, and RFs only selected 30 wavelengths for inputs to the models, which may not be enough to account for all the variability in the samples. Regarding the algorithms evaluated in this study, DTs and RFs successively apply rules to individual wavelengths and therefore do not use the full wavelength at each decision node. The most important wavelengths determined by the RF algorithm were in the range 2028–2064 nm (Table 5). Although, the wavelengths do not correlate to a specific peak, they are most likely associated with the adjacent peak located at 2100–2200 nm associated with long-chain fatty acids (Vitelli et al., 2021; Li et al., 2020). This peak was present for the whole egg powder, egg yolk powder, powdered peanut butter, peanut flour, coconut flour and almond flour. The second most

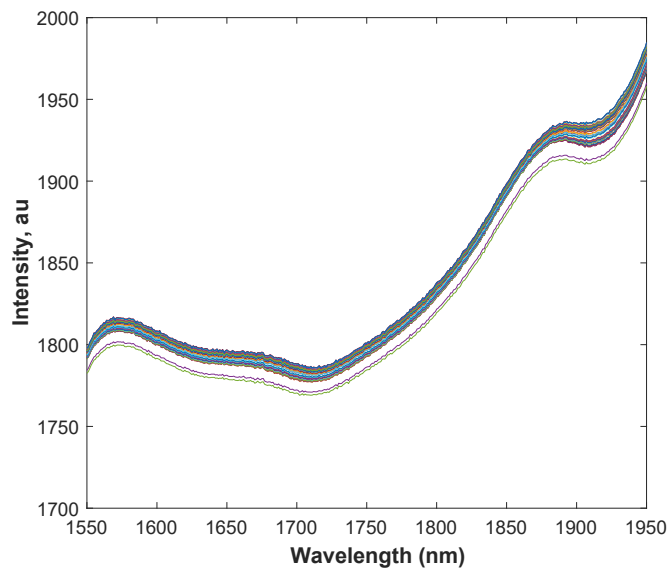


Fig. 6. AEs pre-processed NIR spectra (50) of rye flour acquired from S2.0 sensor at static mode.

important peaks were located in the range 2307–2312 nm which are in the range of the water absorption peak located from 2210 to 2400 nm and present in most materials (Pu et al., 2021; Vitelli et al., 2021; Mishra et al., 2015). Finally, ANNs transform the input spectra into new features which may have led to overfitting compared with using the original spectra. Furthermore, the principle behind KNNs and SVMs, which classify samples based on distances between feature distributions, may have made these algorithms more able to generalize to the 50% of validation set. Therefore, these features and algorithm combinations were taken forward to evaluate ML models on the test set and to evaluate models using the data from both sensors.

4.3. Accuracy of ML algorithms on the test set

To combine sensor data using the CNNs, the network weights pre-trained on the individual sensor data were used to extract features after the final max pooling layer for input into KNN and SVM models. Overall, SVM models using the combined data from both sensors achieved the highest accuracy of 0.9936 and 0.9952 for 2 out of 4 samples at static mode (bolded in Table 6). Therefore, these methods were used to produce the final models. Previous studies have also shown the highest accuracy values were obtained from SVM models for classification and prediction of food powders using NIR spectra (Mohamed et al., 2019). Similar to the ANNs, the features extracted by the CNNs may have led to overfitting and therefore their decreased accuracy compared with the SVMs. Additionally, SVMs may have achieved higher accuracy than KNN due to their ability to use all samples from a material category to determine classification boundaries, compared with KNNs which only use a small number of nearest neighbours to the data point. Table 6 shows the evaluation of the ML models on the test dataset accuracy. This table includes the optimized ML models, CNN models, and models using data from both sensors combined. Spectra acquired from each sample in static mode produced higher accuracy models compared with the moving samples, for all single sensor and combined ML algorithms (Table 6). The results indicate that increasing sample speed resulted in reductions in prediction accuracy for all models most likely due to the increase in variance of recorded spectra from the sensors under moving conditions along with a reduction in intensity of spectral peaks (Dixit et al., 2016; Cama-Moncunill et al., 2016). Combining measurements from both sensors produced the most accurate models, producing the highest, or joint highest, accuracy for 2 out of 4 sample speeds by using KNNs and SVMs (Table 6). This indicates that a wider wavelength range is required for accurate identification of the food powders over that available from a single sensor. Comparing the performance accuracies of ML models which used the normalized NIR

Spectra acquired from both the S2.0 and S2.5 sensors (Table 6), S2.0 produced higher accuracy than S2.5 for static mode and all speeds. This may be due to more absorption peaks of the main chemical components in the food samples being present in the wavelength range of S2.0 sensor (Fig. 3a).

4.4. Under-sampling and boosting

Finally, to improve overall model accuracy, improve model accuracy on difficult to categorize materials, and provide a measure of model confidence, under-sampling and boosting were used. Two models were trained: firstly, a model was trained on the training set and evaluated on the validation set. Secondly, a model was trained on the validation set and evaluated using the training set. The materials that were classified with 100% accuracy were then identified. The under-sampling method halved the dataset size for these materials in their respective training sets. The models were retrained using the new datasets which enabled a larger influence on the more difficult to categorize materials during the 2-fold Bayesian optimization procedure. The correctly classified materials were again identified. Using knowledge of the correctly classified materials from the evaluation of these four models, the under-sampling

approach was applied to the full training and validation set. This produced, in total, five training sets for evaluation on the test set. A SVM model using the combined sensor data was trained on each of these test sets and the predictions aggregated in an ensemble through majority voting. The ensemble method marginally increased in model accuracy for 3 out of 4 speeds along with providing a measure of model confidence (Table 7). In practice, this method can be extended to ensemble sizes much greater than five classifiers.

To determine the materials which were the most difficult to classify between, the misclassified materials for the test set and S2.0 sensor at 0.068 m s⁻¹ and boosting are presented in Table 8.

There was 52 misclassified materials and 27 of these were between Rye flour and Barley Flour. Although the composition of these materials was different (Supplementary Material Table 1) their measured NIR spectra were similar (spectral similarity 0.01 - Supplementary Table 5), which is most likely the reason for the misclassification. Ten of the other misclassified materials were grain based flours, which also had similarities in their recorded NIR spectra (spectral similarity all <0.1 - Supplementary Table 5). In terms of misclassification between the different groups of powdered materials (Flours Containing Gluten, Gluten-Free Flours, Nut Flours, Animal-Based Powders - Table 1) only 8 of the 52 misclassified materials were across groups with the most frequent occurrences (6) involving peanut butter powder.

4.5. Independent training and validation

The final models were then evaluated on the independent samples within the dataset as shown in Table 9. As spectra were collected from five independent samples of each material, the training and validation set could contain a minimum of 40% of the data (corresponding to two independent samples) and the test set could contain a minimum of 20% of the data (corresponding to one independent sample). Compared with the results presented in Table 7, it can be seen that there is a reduction in prediction accuracy when using a similarly sized training, validation, and test split (i.e., 50% compared with 40 or 60%). However, once 80% of the data is used for training and validation, the prediction accuracy rises above the previously reported results in Table 7. This shows that sample collection and preparation methods do have an impact on the acquired spectra which possibly originates from differences in the sample material or differences in the method of sample compaction.

5. Conclusions

This study illustrates the potential of low cost, low power NIR sensors combined with ML methods to classify food powder materials under moving conditions. This could be used to eliminate errors within food production environments and maintain product safety. Overall, accuracies of 99.52, 97.12, 94.08, and 91.68% accuracy for the static, 0.017, 0.036 and 0.068 m s⁻¹ sample speeds were achieved. This was using autoencoders for spectral pre-processing, all spectra wavelengths for both NIR sensors, and support vector machines. Interestingly, CNNs did not produce the most accurate predictions most likely due to overfitting on the 50% training dataset split. The classification accuracy decreased with increasing sample speed most likely due to increased noise and a reduction in spectral peak intensities caused by the motion conditions. Future work will focus on transfer ML models from static conditions to motion conditions using transfer learning and domain adaptation.

Credit author statement

Samet Ozturk: Designing experimental methodology, conceptualizing the content, performing experiment and writing the manuscript. **Alexander Bowler:** Performing machine learning models and writing manuscript. **Ahmed Rady:** Conceptualizing the content and reviewing the manuscript. **Nicholas J Watson:** Conceptualizing the content, designing the experimental methodology, supervising, funding

acquisition, reviewing and editing the manuscript.

Declaration of competing interest

The authors declare that they have no conflict of interest.

Data availability

Data will be made available on request.

Acknowledgment

The authors gratefully acknowledge the financial support provided by the University of Nottingham STFC Impact Acceleration Account and the University of Nottingham Smart Products Beacon of Excellence.

Appendix A. Supplementary data

Supplementary data to this article can be found online at <https://doi.org/10.1016/j.jfoodeng.2022.111339>.

References

- Adeawale, P., Mba, O., Dumont, M.J., Ngadi, M., Cocciardi, R., 2014. Determination of the iodine value and the free fatty acid content of waste animal fat blends using FT-NIR. *Vib. Spectrosc.* 72, 72–78. <https://doi.org/10.1016/j.vibspec.2014.02.016>.
- Avila, N.F., Figueroa, G., Chu, C.C., 2018. NTL detection in electric distribution systems using the maximal overlap discrete wavelet-packet transform and random under sampling boosting. *IEEE Trans. Power Syst.* 33 (6), 7171–7180. <https://doi.org/10.1109/TPWRS.2018.2853162>.
- Cama-Moncunill, R., Markiewicz-Keszycza, M., Dixit, Y., Cama-Moncunill, X., Casado-Gavaldá, M.P., Cullen, P.J., Sullivan, C., 2016. Multipoint NIR spectroscopy for gross composition analysis of powdered infant formula under various motion conditions. *Talanta* 154, 423–430. <https://doi.org/10.1016/j.talanta.2016.03.084>.
- Campbell, J.F., Arbogast, R.T., 2004. Stored-product insects in a flour mill: population dynamics and response to fumigation treatments. *Entomol. Exp. Appl.* 112 (3), 217–225. <https://doi.org/10.1111/j.0013-8703.2004.00197.x>.
- Chandler, M., Jenkins, C., Shermer, S.M., Langbein, F.C., 2019. MRSNet: Metabolite Quantification from Edited Magnetic Resonance Spectra with Convolutional Neural Networks. <https://doi.org/10.48550/arXiv.1909.03836>. *arXiv preprint arXiv:1909.03836*.
- Chen, Y.Y., Wang, Z.B., 2019a. End-to-end quantitative analysis modeling of near-infrared spectroscopy based on convolutional neural network. *J. Chemometr.* 33 (5), e3122. <https://doi.org/10.1002/cem.3122>.
- Chen, Y.Y., Wang, Z.B., 2019b. Feature selection based convolutional neural network pruning and its application in calibration modeling for NIR spectroscopy. *Chemometr. Intell. Lab. Syst.* 191, 103–108. <https://doi.org/10.1016/j.chemolab.2019.06.004>.
- Chen, H., Chen, A., Xu, L., Xie, H., Qiao, H., Lin, Q., Cai, K., 2020. A deep learning CNN architecture applied in smart near-infrared analysis of water pollution for agricultural irrigation resources. *Agric. Water Manag.* 240, 106303. <https://doi.org/10.1016/j.agwat.2020.106303>.
- Corro-Herrera, V.A., Gómez-Rodríguez, J., Hayward-Jones, P.M., Barradas-Dermitz, D. M., Aguilar-Uscanga, M.G., Gschaedler-Mathis, A.C., 2016. In-situ monitoring of *Saccharomyces cerevisiae* ITV 01 bioethanol process using near-infrared spectroscopy NIRs and chemometrics. *Biotechnol. Prog.* 32 (2), 510–517. <https://doi.org/10.1002/btpr.2222>.
- Cui, C., Fearn, T., 2018. Modern practical convolutional neural networks for multivariate regression: applications to NIR calibration. *Chemometr. Intell. Lab. Syst.* 182, 9–20. <https://doi.org/10.1016/j.chemolab.2018.07.008>.
- Damez, J.L., Clerjon, S., 2013. Quantifying and predicting meat and meat products quality attributes using electromagnetic waves: an overview. *Meat Sci.* 95 (4), 879–896. <https://doi.org/10.1016/j.meatsci.2013.04.037>.
- Dixit, Y., Casado-Gavaldá, M.P., Cama-Moncunill, R., Cama-Moncunill, X., Cullen, P.J., Sullivan, C., 2016. Prediction of beef fat content simultaneously under static and motion conditions using near infrared spectroscopy. *J. Near Infrared Spectrosc.* 24 (4), 353–361. <https://doi.org/10.1255/jnirs.1221>.
- Dixit, Y., Casado-Gavaldá, M.P., Cama-Moncunill, R., Cama-Moncunill, X., Markiewicz-Keszycza, M., Cullen, P.J., Sullivan, C., 2017. Developments and challenges in online NIR spectroscopy for meat processing. *Compr. Rev. Food Sci. Food Saf.* 16 (6), 1172–1187. <https://doi.org/10.1111/1541-4337.12295>.
- dos Santos Pereira, E.V., de Sousa Fernandes, D.D., de Araújo, M.C.U., Diniz, P.H.G.D., Maciel, M.I.S., 2021. In-situ authentication of goat milk in terms of its adulteration with cow milk using a low-cost portable NIR spectrophotometer. *Microchem. J.* 163, 105885. <https://doi.org/10.1016/j.microc.2020.105885>.
- Einarson, K.A., Baum, A., Olsen, T.B., Larsen, J., Armagan, I., Santacoloma, P.A., Clemmensen, L.K., 2022. Predicting pectin performance strength using near-infrared spectroscopic data: a comparative evaluation of 1-D convolutional neural network, partial least squares, and ridge regression modeling. *J. Chemometr.* 36 (2), e3348. <https://doi.org/10.1002/cem.3348>.
- ElMasry, G., Wold, J.P., 2008. High-speed assessment of fat and water content distribution in fish fillets using online imaging spectroscopy. *J. Agric. Food Chem.* 56, 7672–7677. <https://doi.org/10.1021/jf801074s>.
- Escrib, J., Woolley, E., Rangappa, S., Simeone, A., Watson, N.J., 2019. Clean- in-place monitoring of different food fouling materials using ultrasonic measurements. *Food Control* 104, 358–366. <https://doi.org/10.1016/j.foodcont.2019.05.013>.
- Escrib, J., Woolley, E., Simeone, A., Watson, N.J., 2020. Monitoring the cleaning of food fouling in pipes using ultrasonic measurements and machine learning. *Food Control* 116, 107309. <https://doi.org/10.1016/j.foodcont.2020.107309>.
- Feng, X., Zhang, Q., Cong, P., Zhu, Z., 2013. Preliminary study on classification of rice and detection of paraffin in the adulterated samples by Raman spectroscopy combined with multivariate analysis. *Talanta* 115, 548–555. <https://doi.org/10.1016/j.talanta.2013.05.072>.
- FSA, (Food Standard Agency), 2020. Business Committee Meeting – September 2020. Available online: <https://www.food.gov.uk/sites/default/files/media/document/fsa-a-20-09-12-incidents-resilience-annual-report.pdf>. (Accessed 4 April 2022). Accessed on.
- Galvin-King, P., Haughey, S.A., Elliott, C.T., 2021. Garlic adulteration detection using NIR and FTIR spectroscopy and chemometrics. *J. Food Compos. Anal.* 96, 103757. <https://doi.org/10.1016/j.jfca.2020.103757>.
- Kawamura, K., Nishigaki, T., Andriamananjara, A., Rakotonindrina, H., Tsujimoto, Y., Moritsuka, N., Rabenarivo, M., et al., 2021. Using a one-dimensional convolutional neural network on visible and near-infrared spectroscopy to improve soil phosphorus prediction in Madagascar. *Rem. Sens.* 13 (8), 1519. <https://doi.org/10.3390/rs13081519>. MDPI AG.
- Khalid, S., Khalil, T., Nasreen, S., 2014. A survey of feature selection and feature extraction techniques in machine learning. *IEEE* 372–378. <https://doi.org/10.1109/SAI.2014.6918213>. August 2014 Science and Information Conference.
- Kosmowski, F., Worku, T., 2018. Evaluation of a miniaturized NIR spectrometer for cultivar identification: the case of barley, chickpea and sorghum in Ethiopia. *PLoS One* 13 (3), e0193620. <https://doi.org/10.1371/journal.pone.0193620>.
- Krauß, W., Bremer, S., Wardekker, J.A., Marschütz, B., Baztan, J., da Cunha, C., 2018. Initial mapping of narratives of change. https://cocliserv.cearc.fr/sites/cocliserv.cearc.fr/files/resultats/CoCliServ_D1.1.pdf. (Accessed 3 October 2022).
- Laborde, A., Jaillais, B., Roger, J.-M., Metz, M., Pouveresse, D.J.-R., Eveleigh, L., Cordella, C., 2020. Subpixel detection of peanut in wheat flour using a matched subspace detector algorithm and near-infrared hyperspectral imaging. *Talanta* 216. <https://doi.org/10.1016/j.talanta.2020.120993>.
- Li, R., Kawamura, S., Fujita, H., Fujikawa, S., 2013. Near-infrared spectroscopy for determining grain constituent contents at grain elevators. *Eng. Agric. Environ. Food* 6, 20–26. [https://doi.org/10.1016/S1881-8366\(13\)80013-4](https://doi.org/10.1016/S1881-8366(13)80013-4).
- Li, X., Zhang, L., Zhang, Y., Wang, D., Wang, X., Yu, L., et al., 2020. Review of NIR spectroscopy methods for nondestructive quality analysis of oilseeds and edible oils. *Trends Food Sci. Technol.* 101, 172–181. <https://doi.org/10.1016/j.tifs.2020.05.002>.
- Liu, Y., Zhou, S., Han, W., Li, C., Liu, W., Qiu, Z., Chen, H., 2021. Detection of adulteration in infant formula based on ensemble convolutional neural network and near-infrared spectroscopy. *Foods* 10 (4), 785. <https://doi.org/10.3390/foods10040785>. MDPI AG.
- Lohumi, S., Lee, S., Lee, W.H., Kim, M.S., Mo, C., Bae, H., Cho, B.K., 2014. Detection of starch adulteration in onion powder by FT-NIR and FT-IR spectroscopy. *J. Agric. Food Chem.* 62 (38), 9246–9251. <https://doi.org/10.1021/jf500574m>.
- Lussier, F., Missirlis, D., Spatz, J.P., Masson, J.F., 2019. Machine-learning-driven surface-enhanced Raman scattering optophysiology reveals multiplexed metabolite gradients near cells. *ACS Nano* 13 (2), 1403–1411. <https://doi.org/10.1021/acsnano.8b07024>.
- Ma, T., Wang, S., Xia, Y., Zhu, X., Evans, J., Sun, Y., He, S., 2021. CNN-based classification of fNIRS signals in motor imagery BCI system. *J. Neural. Eng.* 18 (5). <https://doi.org/10.1088/1741-2552/abf187>. 10.1088/1741-2552/abf187.
- Mateo, M.J., O'Callaghan, D.J., Everard, C.D., Castillo, M., Payne, F.A., O'Donnell, C.P., 2010. Evaluation of on-line optical sensing techniques for monitoring curd moisture content and solids in whey during syneresis. *Food Res. Int.* 43 (1), 177–182. <https://doi.org/10.1016/j.foodres.2009.09.023>.
- Mishra, P., Passos, D., 2021. A synergistic use of chemometrics and deep learning improved the predictive performance of near-infrared spectroscopy models for dry matter prediction in mango fruit. *Chemometr. Intell. Lab. Syst.* 212, 104287. <https://doi.org/10.1016/j.chemolab.2021.104287>.
- Mishra, P., Herrero-Langreo, A., Barreiro, P., Roger, J.M., Diezma, B., Gorretta, N., Lleó, L., 2015. Detection and quantification of peanut traces in wheat flour by near infrared hyperspectral imaging spectroscopy using principal-component analysis. *J. Near Infrared Spectrosc.* 23 (1), 15–22. <https://doi.org/10.1255%2Fjnirs.1141>.
- Modupalli, N., Naik, M., Sunil, C.K., Natarajan, V., 2021. Emerging non-destructive methods for quality and safety monitoring of spices. *Trends Food Sci. Technol.* 108, 133–147. <https://doi.org/10.1016/j.tifs.2020.12.021>.
- Mohamed, M.Y., Solihin, M.I., Astuti, W., Ang, C.K., Zailah, W., 2019. Food powders classification using handheld near-infrared spectroscopy and support vector machine. *J. Phys. Conf.* 1367 (1), 012029. <https://doi.org/10.1088/1742-6596/1367/1/012029>. IOP Publishing.
- Munir, M.T., Wilson, D.I., Depree, N., Boiarkina, I., Prince-Pike, A., Young, B.R., 2017. Real-time product release and process control challenges in the dairy milk powder industry. *Curr. Opin. Food Sci.* 17, 25–29. <https://doi.org/10.1016/j.cofs.2017.08.005>.

- Napoletano, P., Piccoli, F., Schettini, R., 2018. Anomaly detection in nanofibrous materials by CNN-based self-similarity. *Sensors* 18 (1), 209. <https://doi.org/10.3390/s18010209>.
- Ng, W., Minasny, B., McBratney, A., 2020. Convolutional neural network for soil microplastic contamination screening using infrared spectroscopy. *Sci. Total Environ.* 702, 134723 <https://doi.org/10.1016/j.scitotenv.2019.134723>.
- Patel, H., Upla, K.P., 2022. A shallow network for hyperspectral image classification using an autoencoder with convolutional neural network. *Multimed. Tool. Appl.* 81 (1), 695–714. <https://doi.org/10.1007/s11042-021-11422-w>.
- Pauli, Michelle, Kanza, Samantha, Frey, Jeremy G., Brewer, Stephen, 2020. AI3SD & IoT AI for Allergen Detection and Smart Cleaning within Food Production Workshop Report 2019 (AI3SD-Event-Series, 14. In: Jonathan (Ed.), vol. 7. University of Southampton. <https://doi.org/10.5258/SOTON/P0019>.
- Pedreschi, F., Segtnan, V.H., Knutsen, S.H., 2010. On-line monitoring of fat, dry matter and acrylamide contents in potato chips using near infrared interreflectance and visual reflectance imaging. *Food Chem.* 121 (2), 616–620. <https://doi.org/10.1016/j.foodchem.2009.12.075>.
- Porep, J.U., Kammerer, D.R., Carle, R., 2015. On-line application of near infrared (NIR) spectroscopy in food production. *Trends Food Sci. Technol.* 46 (2), 211–230. <https://doi.org/10.1016/j.tifs.2015.10.002>.
- Pu, Y., Pérez-Marín, D., O'Shea, N., Garrido-Varo, A., 2021. Recent advances in portable and handheld NIR spectrometers and applications in milk, cheese and dairy powders. *Foods* 10 (10), 2377. <https://doi.org/10.3390/foods10102377>.
- Rady, A., Fischer, J., Reeves, S., Logan, B., James Watson, N., 2019. The effect of light intensity, sensor height, and spectral pre-processing methods when using NIR spectroscopy to identify different allergen-containing powdered foods. *Sensors* 20 (1), 230. <https://doi.org/10.3390/s20010230>.
- Rinnan, Å., Van Den Berg, F., Engelsen, S.B., 2009. Review of the most common pre-processing techniques for near-infrared spectra. *TrAC, Trends Anal. Chem.* 28 (10), 1201–1222. <https://doi.org/10.1016/j.trac.2009.07.007>.
- Rodriguez-Galiano, V., Sanchez-Castillo, M., Chica-Olmo, M., Chica-Rivas, M.J.O.G.R., 2015. Machine learning predictive models for mineral prospectivity: an evaluation of neural networks, random forest, regression trees and support vector machines. *Ore Geol. Rev.* 71, 804–818. <https://doi.org/10.1016/j.oregeorev.2015.01.001>.
- Sadeghi Vasafi, P., Hitzmann, B., 2021. Comparison of various classification techniques for supervision of milk processing. *Eng. Life Sci.* <https://doi.org/10.1002/elsc.202100098>.
- Salguero-Chaparro, L., Baeten, V., Fernández-Pierna, J.A., Peña-Rodríguez, F., 2013. Near infrared spectroscopy (NIRS) for on-line determination of quality parameters in intact olives. *Food Chem.* 139 (1–4), 1121–1126. <https://doi.org/10.1016/j.foodchem.2013.01.002>.
- Sharma, V., Chauhan, R., Kumar, R., 2021. Spectral characteristics of organic soil matter: a comprehensive review. *Microchem. J.* 171, 106836 <https://doi.org/10.1016/j.microc.2021.106836>.
- Silva, J.G.S., Carames, E.T.D., Pallone, J.A.L., 2021. Additives and soy detection in powder rice beverage by vibrational spectroscopy as an alternative method for quality and safety control. *LWT—Food Sci. Technol.* 137 <https://doi.org/10.1016/j.lwt.2020.110331>.
- Smola, A.J., Schölkopf, B., 2004. A tutorial on support vector regression. *Stat. Comput.* 14 (3), 199–222. <https://doi.org/10.1023/B:STCO.0000035301.49549.88>.
- Su, W.H., Sun, D.W., 2017. Evaluation of spectral imaging for inspection of adulterants in terms of common wheat flour, cassava flour and corn flour in organic Avatar wheat (*Triticum spp.*) flour. *J. Food Eng.* 200, 59–69. <https://doi.org/10.1016/j.jfoodeng.2016.12.014>.
- Su, W.H., Sun, D.W., 2018. Fourier transform infrared and Raman and hyperspectral imaging techniques for quality determinations of powdery foods: a review. *Compr. Rev. Food Saf.* 17 (1), 104–122. <https://doi.org/10.1111/1541-4337.12314>.
- Teena, M.A., Manickavasagan, A., Ravikanth, L., Jayas, D.S., 2014. Near infrared (NIR) hyperspectral imaging to classify fungal infected date fruits. *J. Stored Prod. Res.* 59, 306–313. <https://doi.org/10.1016/j.jspr.2014.09.005>.
- Tegegn, D.D., Zoppis, I.F., Manzoni, S., Sas, C., Lotti, E., 2021. Convolutional Neural Networks for Quantitative Prediction of Different Organic Materials Using Near-Infrared Spectrum.
- Temmerman, J. de, Saeys, W., Nicolai, B., Ramon, H., 2007. Near infrared reflectance spectroscopy as a tool for the in-line determination of the moisture concentration in extruded semolina pasta. *Biosyst. Eng.* 97, 313–321. <https://doi.org/10.1016/j.biosystemseng.2007.03.020>.
- Tsakiridis, N.L., Keramaris, K.D., Theocharis, J.B., Zalidis, G.C., 2020. Simultaneous prediction of soil properties from VNIR-SWIR spectra using a localized multi-channel 1-D convolutional neural network. *Geoderma* 367, 114–208. <https://doi.org/10.1016/j.geoderma.2020.114208>.
- Vitelli, M., Mehtash, H., Assatory, A., Tabtabaei, S., Legge, R.L., Rajabzadeh, A.R., 2021. Rapid and non-destructive determination of protein and starch content in agricultural powders using near-infrared and fluorescence spectroscopy, and data fusion. *Powder Technol.* 381, 620–631. <https://doi.org/10.1016/j.powtec.2020.12.030>.
- Wang, Y., Li, M., Ji, R., Wang, M., Zheng, L., 2020. Comparison of soil total nitrogen content prediction models based on Vis-NIR spectroscopy. *Sensors* 20 (24), 7078. <https://doi.org/10.3390/s20247078>.
- Wang, Z., Wu, Q., Kamruzzaman, M., 2022. Portable NIR spectroscopy and PLS based variable selection for adulteration detection in quinoa flour. *Food Control.* <https://doi.org/10.1016/j.foodcont.2022.108970>, 108970.
- Xia, Y., Huang, W., Fan, S., Li, J., Chen, L., 2018. Effect of fruit moving speed on online prediction of soluble solids content of apple using Vis/NIR diffuse transmission. *J. Food Process. Eng.* 41 (8), e12915 <https://doi.org/10.1111/jfpe.12915>.
- Xu, H., Qi, B., Sun, T., Fu, X., Ying, Y., 2012. Variable selection in visible and near-infrared spectra: application to on-line determination of sugar content in pears. *J. Food Eng.* 109, 142–147. <https://doi.org/10.1016/j.jfoodeng.2011.09.022>.
- Yan, X., Fu, H., Zhang, S., Qu, H., 2020. Combining convolutional neural networks and in-line near-infrared spectroscopy for real-time monitoring of the chromatographic elution process in commercial production of notoginseng total saponins. *J. Separ. Sci.* 43 (3), 663–670. <https://doi.org/10.1002/jssc.201900874>.
- Yang, X.S., Wang, L.L., Zhou, X.R., Shuang, S.M., Zhu, Z.H., Li, N., et al., 2013. Determination of protein, fat, starch, and amino acids in foxtail millet [*Setaria italica* (L.) Beauv.] by Fourier transform near-infrared reflectance spectroscopy. *Food Sci. Biotechnol.* 22 (6), 1495–1500. <https://doi.org/10.1007/s10068-013-0243-1>.
- You, H., Kim, Y., Lee, J.H., Choi, S., 2017. Classification of food powders using handheld NIR spectrometer. 2017 Ninth International Conference on Ubiquitous and Future Networks (ICUFN) 732–734. <https://doi.org/10.1109/ICUFN.2017.7993887>. IEEE.
- You, H., Kim, H., Joo, D.K., Lee, S.M., Kim, J., Choi, S., 2019. Classification of food powders with open set using portable vis-nir spectrometer. 2019 International Conference on Artificial Intelligence in Information and Communication (ICAIC) 423–426. <https://doi.org/10.1109/ICAIC.2019.8668992>. IEEE.
- Zamora-Rojas, E., Pérez-Marín, D., De Pedro-Sanz, E., Guerrero-Ginel, J.E., Garrido-Varo, A., 2012. Handheld NIRS analysis for routine meat quality control: database transfer from at-line instruments. *Chemometr. Intell. Lab. Syst.* 114, 30–35. <https://doi.org/10.1016/j.chemolab.2012.02.001>.
- Zhang, S., Tan, Z., Liu, J., Xu, Z., Du, Z., 2020. Determination of the food dye indigotine in cream by near-infrared spectroscopy technology combined with random forest model. *Spectrochim. Acta Mol. Biomol. Spectrosc.* 227, 117551 <https://doi.org/10.1016/j.saa.2019.117551>.
- Zhou, D., Yu, Y., Hu, R., Li, Z., 2020. Discrimination of *Tetrastigma hemsleyanum* according to geographical origin by near-infrared spectroscopy combined with a deep learning approach. *Spectrochim. Acta Mol. Biomol. Spectrosc.* 238, 1183. <https://doi.org/10.1016/j.saa.2020.118380>, 80.